Phase structure of soliton molecules

A. Hause, H. Hartwig, B. Seifert, H. Stolz, M. Böhm, and F. Mitschke*
Universität Rostock, Institut für Physik, Rostock, Germany
(Received 7 March 2007; published 29 June 2007)

Temporal optical soliton molecules were recently demonstrated; they potentially allow further increase of data rates in optical telecommunication. Their binding mechanism relies on the internal phases, but these have not been experimentally accessible so far. Conventional frequency-resolved optical gating techniques are not suited for measurement of their phase profile: Their algorithms fail to converge due to zeros both in their temporal and their spectral profile. We show that the VAMPIRE (very advanced method of phase and intensity retrieval of *E*-fields) method performs reliably. With VAMPIRE the phase profile of soliton molecules has been measured, and further insight into the mechanism is obtained.

DOI: 10.1103/PhysRevA.75.063836 PACS number(s): 42.81.Dp, 42.65.Tg, 42.30.Rx

INTRODUCTION

Today's advanced fiber-optic transmission lines make increasing use of so-called dispersion-managed fibers, i.e., fibers in which segments of positive and negative group velocity dispersion alternate periodically. Typically, data are coded in a return to zero (RZ) format in which a short light pulse sits in a time slot several times wider than its width so that neighboring pulse interaction is avoided. Soliton pulses are particularly interesting because they are robust in the presence of perturbations by exploiting the Kerr nonlinearity to balance the fiber's group velocity dispersion. We demonstrated recently both numerically and experimentally that at a certain close spacing two such soliton pulses can form a stable bound state provided they are in antiphase. This compound has been called a soliton molecule [1]. Soliton molecules hold potential for further increasing the data-carrying capacity of fibers by either allowing a much denser packing of signal pulses down to the equilibrium distance of the molecule, or by using nonbinary coding (no pulse=0, single soliton=1, molecule=2, etc.). Note that soliton molecules, being nonlinear entities which have inherited stability from standard solitons, hold the promise to be more robust in the presence of perturbations than other nonbinary but basically linear schemes like quaternary phase shift keying which are currently hotly debated. The potential usefulness of soliton molecules warrants a more detailed study of their properties in general, and their binding mechanism in particular.

As we conducted systematic experiments to further characterize the range of existence and the stability properties of these soliton molecules, it became evident that the core reason for the binding mechanism resides in the phase dynamics inside the pulse. Relative phase is well known to mediate attractive or repulsive interaction between solitons [2,3]. Inspired by the discovery of soliton molecules in [1], Mollenauer and Gordon formulated an analytical model [4] in which the pulse's chirp plays the central role and which confirms the prediction of a stable bond at a particular distance.

To get experimental access to phase information, we ventured to measure the full profile (amplitude and phase) of these compounds. In previous art no direct phase information was accessible. Established techniques for amplitude and phase characterization like FROG [5] and its numerous variations [6,7] turn out to be inadequate for assessment of these relatively weak pulses with complex shapes: They not only suffer from ambiguities; the algorithms often tend to stagnate if the temporal and spectral power profiles are highly structured as in this case. The power profile of soliton molecules has a central π phase jump and therefore a central zero; by necessity, the power spectrum then also has zeros.

Interferometric methods like spectral phase interferometry for direct electric-field reconstruction (SPIDER) [8] do not present a viable alternative here because the spectral zeros in the power profile of the soliton molecules are an impediment for this technique, too. SPIDER's phase reconstruction procedure involves a step referred to as "concatenation" [8,9], basically a numerical integration of the derivative of the spectral phase. Since the spectral phase is not defined at zero spectral power points, SPIDER is prone to suffer from undetermined spectral phase jumps, and hence ambiguous temporal profiles. Note that the numerical integration step also used in techniques like measurement of electric field by interferometric spectral trace observation (MEFISTO) [10] and blind MEFISTO [11] causes the same problems.

We present a successful experimental characterization of amplitude and phase profiles of a soliton molecule in an optical fiber by application of the VAMPIRE method (very advanced method of phase and intensity retrieval of *E* fields) invented by Seifert *et al.* [12]. More detail about this method is given below, but first we describe the experimental setup.

SOLITON MOLECULE: EXPERIMENTAL SETUP

As a light source we use an optical parametric oscillator (Mira OPO advanced linear CTA, APE GmbH, Berlin), pumped by a mode-locked Ti:sapphire laser (Mira 900-F, Coherent Inc., Santa Clara). This system was modified for an increased temporal pulse width. The pulse shape is nearly Gaussian with a mild linear chirp, as in $\exp[-(1+iC)t^2/T_0^2]$. The temporal width is $\tau_{\mathrm{FWHM}} \approx 1.763\, T_0 = 250$ fs, and $C \approx 0.41$. The center wavelength is 1595 nm, and the repetition rate is 56 MHz.

*Electronic address: fedor.mitschke@uni-rostock.de; URL: www.physik.uni-rostock.de/optik

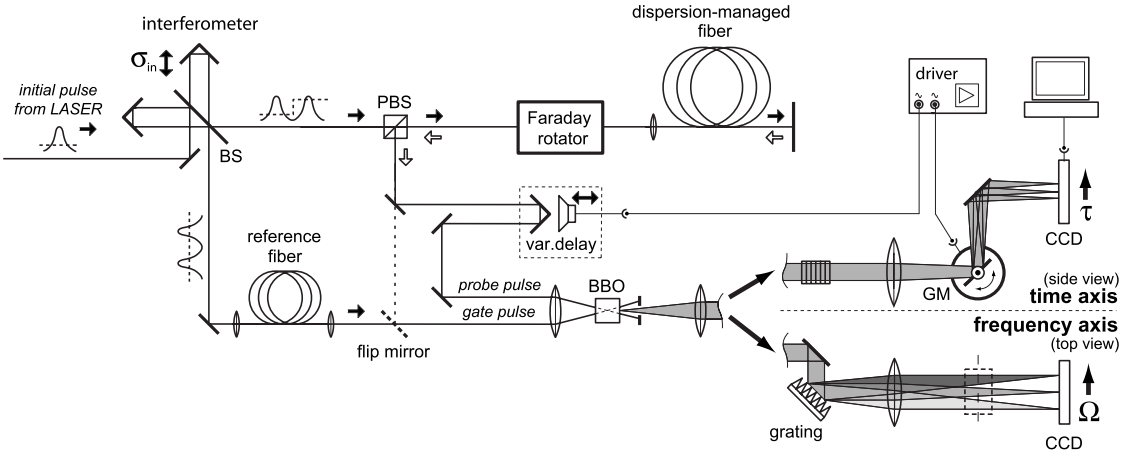

FIG. 1. Experimental setup. BS: beam splitter; PBS: polarizing beam splitter; BBO: nonlinear crystal; GM: galvanometer scanner. The initial pulse is split, delayed, and recombined in the interferometer to generate the double pulse with the desired relative phase and separation. The probe pulse propagates through the dispersion-managed fiber, while the gate pulse propagates through the reference fiber. The BBO crystal generates the cross-correlation signal, and a diffraction grating spectrally disperses it. The spectra are focused on an electronic camera (CCD). The delay axis is swept by a mirror mounted on a galvanometer scanner actuated synchronously with the variable delay of the probe pulse.

The light pulses are sent through a variable attenuator consisting of a half wave plate and polarizing beam splitter to set the desired power level. By way of a Mach-Zehnder interferometer the pulses are split, delayed, and then recombined to form a pulse pair of adjustable temporal separation σ_{in} (see Fig. 1). σ_{in} is precisely known from the path length difference which is a better criterion than distance between maxima, in particular for small distances. A piezoceramic transducer allows us to fine tune the path length difference, and thus both σ_{in} and the relative phase of the pulse pairs. The double pulses taken from one of the interferometer outputs are launched into the dispersion-managed fiber line. (The other output remains unused at this point, but becomes important below.)

In the fiber line segments of normally and anomalously dispersive fiber alternate; the segment lengths are L^+ and L^-, and the line begins and ends with a half-segment of anomalously dispersive fiber. Second order dispersion is not fully compensated so as to give a negative path average dispersion of $\overline{\beta_2}=-2.3$ ps^2/km to support soliton formation. Third order dispersion is nearly compensated by appropriate choice of fiber. The map strength is $S=3.8$ based on the definition

$$S = \frac{|\beta_2^+ - \overline{\beta_2}|L^+ + |\beta_2^- - \overline{\beta_2}|L^-}{\tau_{\mathrm{FWHM}}^2}. \tag{1}$$

Here β_2^+ and β_2^- are the second order dispersion parameters for normally and anomalously dispersive fiber, respectively.

Since the fibers in the line with different dispersion also have different modal area, there are splice losses which limit the useful number of dispersion periods. While in Ref. [1] just three periods were used, we now double this number by using the fiber in a double-pass configuration: At the end of the fiber line, the pulses are reflected back by a mirror so as to pass through it once again in reverse direction. A Faraday rotator before the fiber line rotates the plane of polarization by $\pi/4$, and once again after the second pass. Thus the counterpropagating pulses are orthogonally polarized with respect to the launched pulses and can be coupled out by a polarizing beam splitter.

Six dispersion periods per double-pass correspond to $4.2L_D$, where $L_D=T_0^2/|\overline{\beta_2}|$ is the characteristic dispersion length. This is not a very high value but an improvement over the first demonstration in [1].

Data acquisition involves a spectrometer (not shown in Fig. 1) which provides measurement of spectral power profiles, and a replacement of the autocorrelator used in the first experiment [1], configured in order to allow phase retrieval as described below.

PHASE RETRIEVAL: CHOICES

A variety of techniques exist for full assessment of pulse profiles. FROG is possibly the best-known representative [5], and there are different variations of FROG [6]. The central idea is to measure temporal and spectral information simultaneously in some combined fashion, and then reconstruct the amplitude and phase profiles from the raw data by way of a suitable algorithm. Quite generally all existing techniques show the best results by analysis of more or less simple pulse shapes, such as the output pulses from lasers. More complex amplitude profiles remain problematic for all variations of FROG, in particular when there are zeros or well separated parts in the temporal or spectral domain [7]. In such cases, iterative FROG algorithms [6,13] often do not converge and give meaningless and simply wrong output. Therefore, a reliable full field reconstruction of arbitrary pulse shapes could not be guaranteed by conventional FROG methods.

Of all FROG methods, SHG FROG seems to be the most widely used. Its name is derived from the fact that it uses autocorrelation involving second harmonic generation, its popularity seems to stem from its relative simplicity.

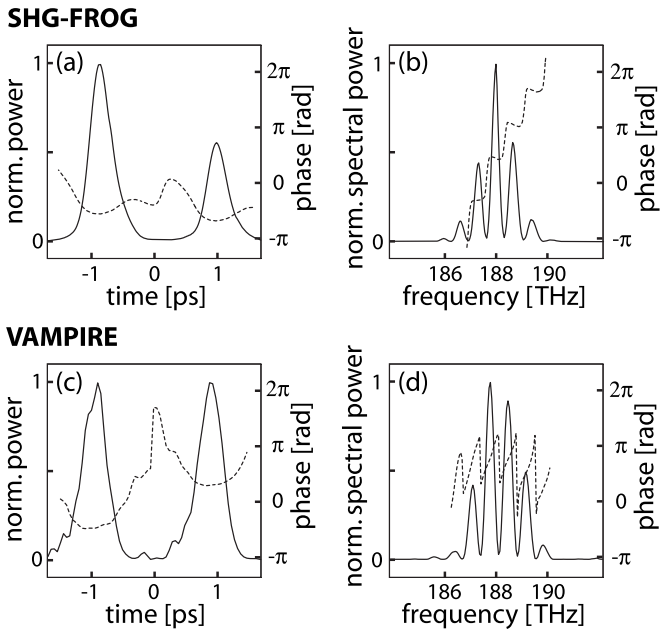

FIG. 2. Reconstructed power profiles and spectra (solid lines), temporal, and spectral phase functions (dashed lines) of an antiphase double pulse. All panels refer to the same experimental conditions. (a) Temporal profile obtained from SHG FROG with conventional reconstruction algorithm. Note that this fails to show a phase jump of π. (b) The complex spectrum retrieved as in (a). This erroneously suggests an in-phase double pulse. (c) Temporal profile obtained from VAMPIRE. This yields the correct pulse shape and temporal phase function. (d) The complex spectrum corresponding to (c), phase retrieved from VAMPIRE, and power profile as measured directly.

Initially we attempted to measure the phase profiles of soliton molecules with SHG FROG. With some minor modifications or extra steps, ambiguities regarding time direction could be avoided, but serious problems arose from the zeros in the spectral profile [7] of the soliton molecules and the concomitant stagnation behavior of the used standard commercial algorithm [14]. A typical reconstruction result from SHG FROG is shown in Fig. 2.

In principle, these problems might be overcome by using a FROG variety based on cross-correlation, known as XFROG [6,15]. However, XFROG requires full and detailed knowledge of the reference pulse. Any errors in the assessment of the reference will propagate into the final result. It is not obvious how one would obtain, and how one could verify, such a reference pulse. Therefore, the use of XFROG is not practical here. Moreover, there is no guarantee that this technique solves the stagnation problem of the reconstruction algorithm.

Then there is blind FROG [6,13]. This is another cross-correlation technique which—as the name suggests—does not require any advance knowledge of the shape of either the pulse to be measured or the reference pulse. It can operate with arbitrary fields $E_1(t)$ and $E_2(t)$. In practical terms, blind FROG has a huge advantage over XFROG in that no exact knowledge of the reference pulse shape is necessary. Nevertheless, there is no general guarantee that a unique field reconstruction is possible. This remains true even when one employs the additional information about the spectral intensities of both pulses, $|\tilde{E}_1(\omega)|^2$ and $|\tilde{E}_2(\omega)|^2$, obtained from independent measurements [12].

We therefore turned to a technique based on [12] called VAMPIRE. VAMPIRE is derived from blind FROG and is based on cross-correlation of the signal under study with some well chosen but not completely characterized reference pulse. This absence of full specification of the reference pulse is one of the differences between VAMPIRE and techniques like XFROG.

We turn to a brief description of the VAMPIRE technique. The two signals to be cross-correlated, i.e., signal and reference, are also known as probe pulse and gate pulse. The measured VAMPIRE spectrogram (somewhat of a misnomer, perhaps, since not just a spectrum is plotted, but the term is commonly used nevertheless [7,16]) can be expressed as

$$I(\Omega,\tau) \propto \left| \int_{-\infty}^{\infty} E_{\text{gate}}(t) E_{\text{probe}}(t-\tau) e^{i\Omega t}\, dt \right|^2 \propto \left| \int_{-\infty}^{\infty} \tilde{E}_{\text{probe}}(\omega) \tilde{E}_{\text{gate}}(\Omega-\omega) e^{i\omega\tau}\, d\omega \right|^2, \quad (2)$$

where E and $\tilde{E}$ denote the complex temporal and spectral field, respectively. Ω defines the spectral axis and τ is the delay.

The reason why VAMPIRE can guarantee the uniqueness of full field reconstruction is that $E_{\text{gate}}(t)$ can be chosen such that $I(\Omega,\tau)$ does not suffer from nontrivial ambiguities. Ideally, this would be achieved by a well-separated double pulse structure with an asymmetry in duration, peak power, and chirp of the individual pulses [12]. A sufficient asymmetry is required, but detailed knowledge of the structure is definitely not. For example, a suitable gate pulse could easily be generated by splitting a laser pulse into a pair by means of a Mach-Zehnder interferometer with a dispersive element in one of its arms. This way the VAMPIRE spectrogram would contain two spectrally dispersed signals from the cross-correlations of the probe pulse with the two different components of the gate pulse so that the required noncentrosymmetric spectrogram is obtained [12]. In comparison to other pulse retrieval techniques, the asymmetry thus provided in the cross-correlation contains just that extra amount of information which guarantees a unique relation between the cross-correlated pulses and the spectrogram.

Beyond this procedure to enhance the information content of the spectrogram, there is a different reconstruction algorithm for VAMPIRE which exploits this information to obtain a unique reconstruction. Stagnation is a persisting problem of conventional iterative FROG algorithms [6,13] but is avoided by VAMPIRE [12] in a special way.

The evaluation of the spectrogram begins with a single row of the spectrogram. For a fixed parameter Ω this row can be expressed by

$$I_\Omega(\tau) \propto |\mathcal{F}_{\omega\to\tau}[G_\Omega(\omega)\exp\{i\phi_\Omega(\omega)\}]|^2, \quad (3)$$

where

$$G_\Omega(\omega) = |\tilde{E}_{\text{probe}}(\omega)||\tilde{E}_{\text{gate}}(\Omega - \omega)| \quad (4)$$

and

$$\phi_\Omega(\omega) = \phi_{\text{probe}}(\omega) + \phi_{\text{gate}}(\Omega - \omega). \quad (5)$$

The choice of this first row is arbitrary; one can therefore pick the one with the best signal-to-noise ratio and asymmetry to minimize the risk of stagnation. From this row one finds its spectral phase function $\phi_\Omega(\omega)$ with an additional constant C_Ω by using a Gerchberg-Saxton algorithm [17] or equivalent method. The power spectra $|\tilde{E}_{\text{gate}}(\omega)|^2$ and $|\tilde{E}_{\text{probe}}(\omega)|^2$ are easily obtained by an independent measurement.

Next, one proceeds with a neighboring row and repeats the Gerchberg-Saxton iteration, this time using the phase function from the first row as an initial guess. Then one continues until all rows are covered. This procedure is different from commonly used iterative algorithms in that VAMPIRE treats the spectrogram locally, not globally. This provides the means to check every single row for stagnating behavior: In every Gerchberg-Saxton loop, the error between the intermediate result and the measured data is calculated. After several iterations, rows with a low error are kept, while those with a higher error may be discarded. Discarding questionable data is no big loss since spectrograms are overdetermined. By this procedure, VAMPIRE is not only guaranteed to converge, but the convergence time is reduced drastically with respect to the commonly used PCGP algorithm [6,13]. At this point one arrives at an array of complex values $G(\Omega,\omega)\exp\{i[\phi(\Omega,\omega)+C(\Omega)]\}$. In a second step one can retrieve the spectral phase functions $\phi_{\text{gate}}(\omega)$ and $\phi_{\text{probe}}(\omega)$ from this array. This step has been proven to yield unambiguous, unique results [12]. The arbitrary phases $C(\Omega)$ can be eliminated in this step; only constant and linear phase terms (corresponding to absolute phase and time) trivially remain undetermined. Finally, the complex temporal structure is obtained in a straightforward fashion by Fourier transform.

The key feature of VAMPIRE is that it is not thwarted by zeros in the temporal or spectral power profile. This sets it apart from previous art and makes it the natural choice for situations as described here.

PHASE RETRIEVAL: IMPLEMENTATION

We successfully use a gate pulse which is derived from the unused output of the Mach-Zehnder pulse-splitting interferometer mentioned above. At this secondary output we have a double pulse, and whenever the first output provides antiphase pulse pairs, the secondary output gives in-phase pulse pairs. We send the signal from the secondary output through an auxiliary fiber which serves the double purpose of conditioning filter and delay line. As a delay line, the auxiliary fiber ensures that the signals to be cross-correlated arrive simultaneously. For pulse shaping, it is composed of one segment of fiber with positive β_2 followed by one segment of fiber with negative β_2. A full compensation of dispersion to zero is not desired; rather, a well-chosen undercompensation imparts a particular amplitude and phase profile characterized by a weakly chirped central main peak and strongly chirped adjacent peaks. This power profile serves the purpose of generating a noncentrosymmetric VAMPIRE spectrogram as required.

Both gate and probe pulses are noncollinearly focused into a nonlinear crystal [beta-barium borate, (BBO)], which is part of the cross-correlator setup. There is a variable temporal delay, provided by a retroreflector mounted on the periodically moving membrane of a loudspeaker. The cross-correlation signal is spectrally dispersed with a blazed grating (1200 lines/mm) and focused onto the light-sensitive element of an Apogee AP7 camera. This camera has a cooled CCD chip of 512×512 square pixels of 24 μm pitch. We adjust so that the spectral direction of the VAMPIRE spectrogram is imaged along pixel rows. We then disperse the temporal direction along pixel columns by deflecting the beam with a mirror mounted on a galvanometer scanner (G115, General Scanning, Inc.) which is driven in synchronism with the loudspeaker. It turned out to be difficult to have the images from forward and backward scanning fall onto each other with precision, so we blocked the beam during the backward scan with a mechanical shutter (not shown in Fig. 1).

Different delays between the gate and probe pulses produce characteristic spectra on different rows of the CCD. In the interest of scan linearity, we overdrive the scan range so as to overfill the CCD; this way only the central portion of the sinusoidal motion is used. A complete scan (of which $\approx$30 are taken in a second) maps out a complete 2D image, the VAMPIRE spectrogram as discussed above. The complete information about the complex structure of both probe and gate pulses (signal and reference) is contained in the VAMPIRE spectrogram, waiting to be properly decoded.

For the sake of fair comparison we also recorded conventional SHG FROG signals with the same setup after converting from cross-correlation as described here to autocorrelation, basically by flipping a beam-steering mirror (see Fig. 1).

Projecting all image data onto the temporal axis or frequency axis produces the time or spectral marginal, respectively; these can be useful for calibration and checks. It is necessary to conduct a precise calibration of the spectrogram. A calibration of the spectral axis was done by recording a double pulse SHG FROG spectrogram and adjusting the positional offset and scale factor of its frequency marginal to that of the self-convolution of the independently measured probe pulse spectrum. (If the two do not compare well, the particular data set is discarded). For a calibration of the delay axis a stack of thin glass plates is used, mounted together like a stair so as to provide a stepped thickness. Upon its insertion, a series of equidistant replicas of some test pulse is produced on the camera. This series allows an assessment of scale and nonlinearity of the axis, and based on this information, remaining temporal nonlinearity is removed. Finally, the calibrated image needs to be clipped to 512×512 pixels again so that the digitization steps in temporal and spectral domain ($\Delta\tau$ and $\Delta\Omega$, respectively) fulfill the constraint of $\Delta\tau=2\pi/(512\Delta\Omega)$.

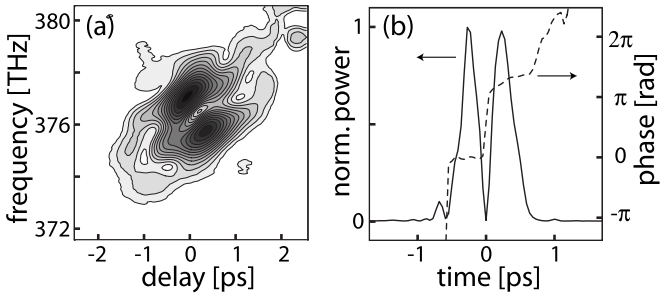

FIG. 3. Example of a characterization of soliton molecules using VAMPIRE. (a) Measured VAMPIRE spectrogram after calibration and linearization as described in the text. (b) Power and phase profile reconstructed from (a). The double-peaked structure with a phase jump of π at the central zero power point, characteristic for a soliton molecule, is clearly evident.

COMPARISON OF SHG-FROG AND VAMPIRE

We recorded a number of spectrograms for each SHG FROG and VAMPIRE. SHG FROG spectrograms were evaluated with a standard commercial reconstruction algorithm [14] and VAMPIRE spectrograms as described above.

SHG FROG was less than successful: The algorithm tended to stagnate due to inherent nontrivial ambiguities [12]. When SHG FROG provided a reconstruction, it was often demonstrably misleading. A typical example is shown in Figs. 2(a) and 2(b). From the independently recorded spectrum we know that there ought to be a central zero, whereas SHG FROG in this case provides a central maximum. Similarly, the temporal profile is just wrong because it does not at all show the central phase jump.

In contrast, phase retrieval using VAMPIRE consistently produced the correct result. Figures 2(c) and 2(d) show the result for the same experimental situation as in Figs. 2(a) and 2(b). It is evident that both the phase jump and the correct position of zeros are reproduced well. Also, the parabolic phase around the power maxima comes out much clearer.

INFORMATION OBTAINED ON SOLITON MOLECULES

In Fig. 3, a measured VAMPIRE spectrogram is shown together with the temporal power and phase profile reconstructed from it. The initial pulse parameters have been chosen so that soliton molecule formation is possible: An antiphase double pulse (initial separation $\sigma_{in}=530$ fs, pulse pair energy 142 pJ) was launched into the fiber line. The data shown represent an average over 10 s exposure time in order to ensure a good signal-to-noise ratio. Care was taken to ensure that parameters were held constant during measurement.

In order to investigate the molecule's stability with respect to parameter variations, and to obtain further insight into the binding mechanism, we varied the initial launch separation σ_{in} from 0.5 ps to 1.5 ps corresponding to 2–6 pulse widths. Phase and power profiles were extracted for each case. Selected results are shown in Fig. 4.

Two vertical dashed lines in the figure denote the soliton molecule's equilibrium separation $\sigma_{out}=0.55$ ps. This separation is found after propagation if σ_{in} is within a certain range, as exemplified by the traces for $\sigma_{in}=0.53$ ps and $\sigma_{in}=0.77$ ps. This is indicative of the stability of the equilibrium separation in the molecule. A pulse pair with a significantly larger initial separation of $\sigma_{in}=1.20$ ps, however, falls outside the capture range for soliton molecule formation. Note that in this case (solid trace) secondary peaks, or at least shoulders, appear at the point of the soliton molecule's equilibrium distance; these have not been predicted or reported before. We will argue that they are indeed to be expected, and that they provide direct insight into the phase structure of the soliton molecules.

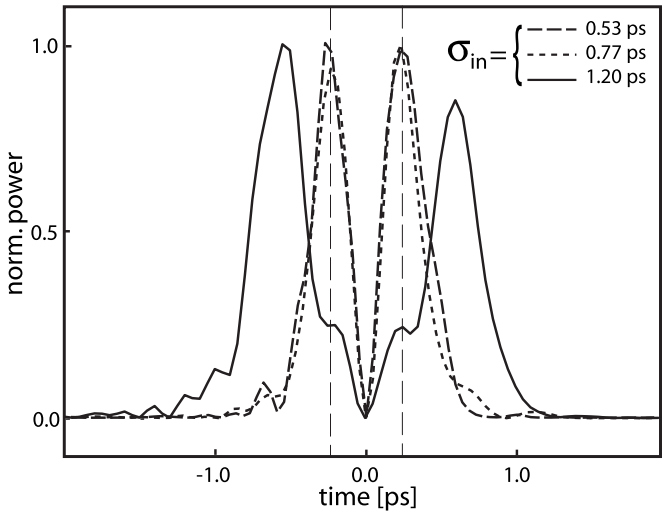

FIG. 4. Typical pulse shapes as reconstructed with VAMPIRE at the end of the fiber line. For values of σ_{in} in the range of 0.53 ps and 0.77 ps, the pulse shapes at the end of the fiber are nearly the same; $\sigma_{out}\approx 0.55$ ps (dashed vertical lines). If σ_{in} is larger (1.20 ps), the main peaks remain at a larger spacing. Note, however, that secondary peaks appear at $\sigma_{out}\approx 0.55$ ps instead.

CHIRP PRODUCES SECONDARY PEAKS

Chirp is easy to describe in very simple cases: In constant-dispersion fiber, solitons are unchirped. In dispersion-managed fiber, their chirp oscillates periodically around zero, with a chirp-free point located at every half-segment [18]. A similar statement holds for soliton molecules. Here, however, we do not restrict ourselves to such simple cases. Rather, propagation of solitons and soliton molecules is subject to splice loss, deviation in pulse shape, mild initial chirp, and different peak powers. At the end of the fiber line we therefore consistently find a considerable chirp in the pulses.

It is a very good approximation to consider dispersion-managed solitons as linearly chirped Gaussian pulses [19,20]. Indeed, we confirmed, in independent measurements not described in detail here but following the same procedures as spelled out above, that individual pulses both from the laser and after fiber propagation are well described by a linearly chirped Gaussian pulse. It is therefore appropriate to treat our double pulses as a superposition of two such Gaussian pulses as shown in Fig. 5. The situation of unchirped

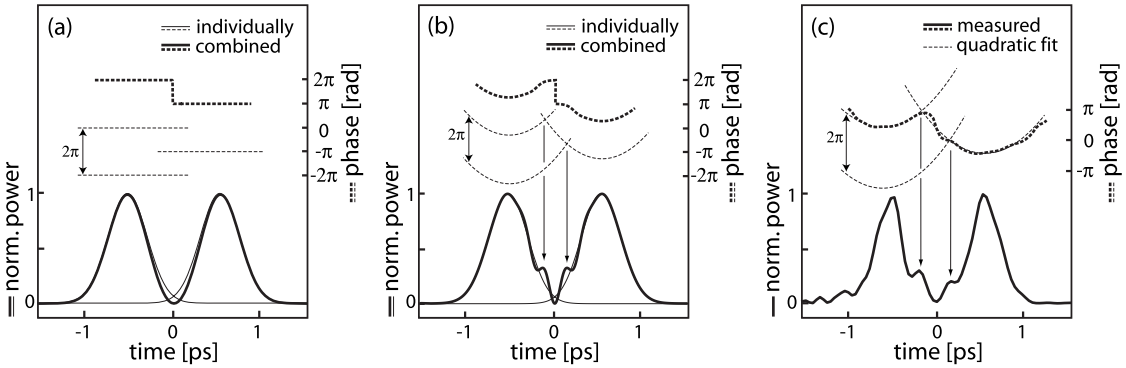

FIG. 5. Comparison of schematic representation and measurement for double pulses generated from superposition of two equal Gaussian pulses. Shown are power (solid) and phase (dashed) profiles. (a) Sketch for the case of two unchirped pulses. Thin lines represent pulses individually; heavy lines represent superposition. Note the constant phases and their resultant (shifted away vertically for clarity). This gives a power profile featuring a central zero with a phase jump of π. (b) Sketch as in (a) but now the pulses are linearly chirped. The phase profiles are parabolic as indicated. Since phase is determined only modulo 2π, one of the parabolas is repeated with a shift of 2π. Constructive interference occurs where parabolas intersect; destructive interference occurs halfway between. Secondary peaks form in the power profile at the locations of constructive interference. (c) Actual measurement, reconstructed with VAMPIRE and to be compared with (b). Quadratic phase functions have been fitted (thin dashed lines) to the reconstructed phase function (heavy dashed line); one of the fits was duplicated with a shift of 2π. The fit is very satisfactory. Secondary peaks appear at the points of constructive interference as described in (b).

pulses [Fig. 5(a)] is particularly easy to understand, but Fig. 5(b) shows that for linearly chirped pulses one expects additional structure in the region of overlap: Constructive interference leads to a local increase of power which takes the form of secondary maxima.

This is exactly what we find in our measurements: Figure 5(c) shows another pulse shape reconstructed with VAMPIRE where the launch separation was several times larger than the equilibrium distance ($\sigma_{\text{in}} \approx 4\tau_{\text{FWHM}}$). Both the position and the height of the secondary peaks agree with the prediction from this model. This strongly suggests that the concept shown in Fig. 5(b) is adequate.

INTERPRETATION

Since the prediction [2] and first observation [3] of interaction forces between solitons, the case of unchirped pulses in fibers with constant dispersion is well understood. The interactive force depends on the relative phase because constructive (destructive) interference produces an intensity enhancement (reduction) which implies an increase (decrease) in local index perturbation by the Kerr effect. Weighting by power at each location in the interaction regime, one obtains as a result that in-phase structures attract, and out-of-phase structures repel, while the overall magnitude of the effect decays with separation of the pulses exponentially, like the power decay in the pulse tails.

We can now apply the same concept to chirped pulses by looking at the phase relation locally. For each position within the pulse pair one gets an interacting force; the overall net effect is found by integration over the whole structure. The net effect can be expected to depend on the pulse pair separation, the pulse width, and the actual chirp. Mollenauer and Gordon have performed this calculation [4] and find that there is net repulsion (attraction) for separations smaller (larger) than a certain equilibrium distance. This implies a stable equilibrium value. Of course, both the values of all forces and the position of this equilibrium oscillate during propagation in the dispersion map, but another integration provides the path average. Indeed they find a path average pulse separation at which there is a stable equilibrium. This corroborates our numerical and experimental results in [1]. Obviously, this simple model has all necessary ingredients to explain the existence of an equilibrium separation, and thus a stable bond between solitons.

However, in our present context the situation is more involved. In the presence of losses, the oscillation of pulse shapes (width, chirp) is not necessarily periodic with the map period. We numerically find situations in which the position of the chirp-free point is not fixed at midsegment, but gradually walks through the map period. Obviously, the configuration of the best stability of the soliton molecule would be obtained when this does not happen; in other words, when the molecule is stroboscopically invariant.

We also know from numerical studies that the chirp in the stroboscopically invariant case is not sufficient to produce the secondary maxima described above. We therefore conclude that longer fiber lines (with loss compensation) would be required to truly differentiate between the fully stable case and the nearly stable situations which appear to be stable in the relatively short fiber line used here.

CONCLUSIONS

It is highly nontrivial to measure the full amplitude and phase profile of complex pulse shapes, in particular when they contain zeros in either temporal or spectral profile, or—as in our case—both. We have shown that conventional SHG FROG does not provide a correct reconstruction; at the same time we could demonstrate that the technique called VAMPIRE is successful.

With VAMPIRE the phase profiles of double peaked pulse shapes were consistently retrieved with success, and gave us useful, previously inaccessible phase information about soliton molecules. At the same time, soliton molecules present a challenge to reconstruction techniques, and VAMPIRE was shown to be successful. Very recently, a mathematical theory was put forward from which the power and phase profiles of soliton molecules can be calculated [21]. This model predicts the existence of a second stable position. We suspect that this finding may be related to the secondary maxima we find in the power profiles. Further research along this line is under way.

ACKNOWLEDGMENTS

This work was supported in the framework of DIP 6.6 (Deutsch-Israelische Projektpartnerschaft). We also acknowledge partial support by Deutsche Forschungsgemeinschaft.

[1] M. Stratmann, T. Pagel, and F. Mitschke, Phys. Rev. Lett. **95**, 143902 (2005).
[2] J. P. Gordon, Opt. Lett. **8**, 596 (1983).
[3] F. Mitschke and L. F. Mollenauer, Opt. Lett. **12**, 355 (1987).
[4] L. F. Mollenauer and J. P. Gordon (private communication).
[5] R. Trebino and D. J. Kane, J. Opt. Soc. Am. A **10**, 1101 (1993).
[6] R. Trebino, *Frequency-Resolved Optical Gating: The Measurement of Ultrashort Laser Pulses* (Kluwer Academic Publishers, Boston, 2002).
[7] D. Keusters, H.-S. Tan, P. O'Shea, E. Zeek, R. Trebino, and W. S. Warren, J. Opt. Soc. Am. B **20**, 2226 (2003).
[8] C. Iaconis and I. A. Walmsley, Opt. Lett. **23**, 792 (1998).
[9] C. Iaconis and I. A. Walmsley, IEEE J. Quantum Electron. **35**, 501 (1999).
[10] I. Amat-Roldan, I. G. Cormack, and P. Loza-Alvarez, Opt. Lett. **30**, 1063 (2005).
[11] I. Amat-Roldan, D. Artigas, I. G. Cormack, and P. Loza-Alvarez, Opt. Express **14**, 4538 (2006).
[12] B. Seifert, H. Stolz, and M. Tasche, J. Opt. Soc. Am. B **21**, 1089 (2004).
[13] D. J. Kane, IEEE J. Quantum Electron. **35**, 421 (1999).
[14] Femtosoft Technologies, Oakland, CA, USA, FROG program v. 3.0.2.
[15] S. Linden, H. Giessen, and J. Kuhl, Phys. Status Solidi B **206**, 119 (1998).
[16] Ch. Dorrer and I. A. Walmsley, EURASIP J. Appl. Signal Processing **2005**, 1541 (2005).
[17] R. W. Gerchberg and W. O. Saxton, Optik (Stuttgart) **35**, 237 (1972).
[18] G. P. Agrawal, *Applications of Nonlinear Fiber Optics* (Academic Press, New York, 2001).
[19] P. M. Lushnikov, Opt. Lett. **26**, 1535 (2001).
[20] L. F. Mollenauer and J. P. Gordon, *Solitons in Optical Fibers: Fundamentals and Applications* (Academic Press, New York, 2006).
[21] I. Gabitov, R. Indik, L. Mollenauer, M. Shkarayev, M. Stepanov, and P. M. Lushnikov, Opt. Lett. **32**, 605 (2007).